CVD Growth of Large-scale and Highly Crystalline 2D Chromium Telluride Nanoflakes

Yuxi Guo[12], Lixing Kang[23], Shaojia Yu[1], Jiefu Yang[2], Xiaofei Qi[1]*, Zhiyong Zhang[1]*, Zheng liu[2]*

1 School of Information Science and Technology, Northwest University, Xi'an, Shaanxi 710127, P. R. China.
2 School of Materials Science and Engineering, Nanyang Technological University, 50 Nanyang Avenue, Singapore 639798, Singapore.
3 Key Laboratory of Multifunctional Nanomaterials and Smart Systems, Division of Advanced Materials, Suzhou Institute of Nano-Tech and Nano-Bionics, Chinese Academy of Sciences, Suzhou 215123, China
*Correspondence: Xiaofei Qi (Email: qixf@nwu.edu.cn), Zhiyong Zhang (Email: zhangzy@nwu.edu.cn) and Zheng Liu (Email: z.liu@ntu.edu.sg)

Keywords: 2D materials, Chromium Telluride, chemical vapor deposition, large-scale synthesis

Abstract

Recently, 2D magnetic materials have attracted much attention due to their potential to apply in spintronic devices. Chromium Telluride (CrTe) flakes has been reported for the hard magnetism with strong perpendicular anisotropy. However, the synthesis of large-scale CrTe nanoflakes on SiO_2/Si substrate is still a challenge. Here, we report the synthesis of large-scale CrTe nanoflakes with the size up to ~250 μm on SiO_2/Si substrate via chemical vapor deposition (CVD) process. Our work demonstrated an effective pathway to synthesize large-scale 2D transition metal tellurides.

Introduction

Two-dimensional (2D) materials have been intensively studied for their unique physical and chemical characteristics. Researchers have discovered many novel 2D atomic-crystal materials ranging from metals, semimetals, semiconductors, superconductors and insulators, which are diverse and complementary in nature. Therefore, 2D materials have penetrated in many existing research fields even developed some new fields, such

as electronics and optoelectronics [1, 2], energy storage [3], sensors [4] and light/electro-catalysts [5]. Furthermore, researchers are committed to explore 2D vdW materials with strong magnetism and high Curie temperatures. In 2016, two separate groups reported antiferromagnetism in 2D $FePS_3$, which provided incontrovertible evidence of an intrinsic magnetic phase transition [6,7]. Subsequently, intrinsic ferromagnetic properties were discovered in exfoliated 2D $Cr_2Ge_2Te_6$ [8]. Layer-dependent ferromagnetism was found in 2D CrI_3 that the single layer CrI_3 shows ferromagnetism while bilayer CrI_3 was antiferromagnetism [9, 10]. Besides, electrically gate-induced ferromagnetic ordering has been achieved in Fe_3GeTe_2 flakes at room-temperature [11]. Bonilla and O'Hara reported room temperature ferromagnetism has been discovered in monolayer VSe_2 [12] and $MnSe_2$ [13], respectively. Recently, authors found that the 2D CrTe flake shows obvious hard magnetic properties with a rectangular hysteresis loop which affected by the thickness [14]. These studies laid the foundation for the study of ferromagnetism based on 2D vdW materials.

Although the great progress has been made in the last few decades, there is still a long way for 2D ferromagnetic materials because the controlled preparation of large-scale uniform 2D materials is still a considerable challenge. Fortunately, chemical vapour deposition (CVD) method is proved to be the most effective way to synthesize large-scale 2D materials with high film quality. Up to now, a large amount of 2D materials with controllable layer number and lateral size have been successfully synthesized *via* CVD methods by precisely controlling the growth parameters, such as precursors, pressure, temperature, heating rate, and substrates. In previous reports, most transition metal dichalcogenides are difficult to be synthesized *via* traditional CVD method due to the high melting points of the primarily precursors (metal powders or metal oxides)., There are two main ways to solve this issue: (1) Using transition metal chlorides (MCl_n) with lower melting points as the metal precursors. The MCl_n precursors can provide a relatively high evaporation rate with high chemical activities, which facilitating the synthesis process. By this CVD strategy, a plenty of 2D transition metal dichalcogenides have been synthesized, such as VSe_2 [15, 16], NbS_2 [17, 18] and $NiTe_2$ [19]. (2) Using mixture of metal oxides (MO_n) and alkali halides as the metal precursors. The

alkali halides will react with metal oxides to form intermediate products, which decrease the melting points of MO_n and increase the overall reaction rates. Zhou et. al reported the systematically synthesis of 47 transition metal dichalcogenides via this salt-assisted CVD method [20]. These two CVD routes have been widely used in growing 2D transition metal dichalcogenides. In addition, it has been reported that tellurium (Te) can lower the melting point of the chemicals. Gong et. al reported that Te can facilitate the synthesis of MoS_2/WS_2 heterojunctions by lowering the melting point of the chemicals, but did not lead to the formation of $MoTe_2$ or WTe_2 flakes [21]. Inspired by this, large-scale and high-quality 2D WTe_2 and $MoTe_2$ were successfully synthesized by using the mixed compounds (WO_3+WCl_6+Te or MoO_3+$MoCl_5$+Te) as metal precursors [22]. This method provides a new idea for synthesis atom-thin transition metal telluride materials.

Here, we demonstrate the synthesis of large-scale CrTe nanoflakes *via* CVD method using the mixed compounds (Cr: $CrCl_3$: Te) as the metal source. The presence of Te powder in metal precursors is conducive to the growth of large-scale CrTe nanoflakes. The as-synthesized CrTe nanoflakes exhibit the largest domain size of ~250 μm on SiO_2/Si substrate. Raman spectroscopy, AFM, STEM, Raman, EDS, XPS and XRD were used to confirm the high quality of the CrTe nanoflakes.

Results and Discussion

The crystal structure of side view and top view of the CrTe are shown in **Figure 1**a. The structure of CrTe belongs to the $P6_3/mmc$ space group with hexagonal NiAs type. The schematic of the CVD setup is depicted in Figure 1b. In this work, tellurium (Te) powder and the mixed compounds (Cr: $CrCl_3 \cdot 6H_2O$: Te) were used as the source of Te and Cr, respectively. Notably, Cr_2O_3 powder is not suitable as a metal precursor because the crystals are extremely hard and stable with a melting point of 2266℃. For high melting point metal oxides, metal chlorides are usually used as substitute precursors since it has low melting point and is easy to evaporate. However, the reaction is too rapid to be controlled if only use $CrCl_3 \cdot 6H_2O$ (melting point < 100℃). Mixed compounds of Cr and $CrCl_3 \cdot 6H_2O$ with an optimized ratio is designed to control

reaction speed to synthesize large-scale CrTe nanoflakes. The Te in the mixed compounds can decrease the melting point of the mixed compounds (the melting point of Cr is 1907℃), which makes metal precursors evaporate more easily to at the growth temperature. The chemical reaction can be described as follows:

$$Cr + 2CrCl_3 + 4Te + 4H_2 \rightarrow 3CrTe + H_2Te\ (g) + 6HCl\ (g) \quad (1)$$

In addition, excessive Te powder in the upstream was used to maintain the Te atmosphere during the whole reaction process, which because Te can be easily carried away by the flow gas during the reaction under high temperature. To a typical reaction, the growing temperature is 700 °C while the growing time is 2 min. The detailed growth information is presented in the Experimental Section.

Figure 2a shows typical optical image of the large single crystalline CrTe nanoflake obtained in 2 min at 700 °C with carrier gas of 100 standard cubic centimeters per minute (sccm) Ar/5 sccm H_2. The lateral size of the as-synthesized CrTe nanoflake is up to ~250 μm. Raman spectra of CrTe nanoflake (Figure 2b) demonstrated two characteristic peaks 123 and 141 cm^{-1}, which consistent with previous reports [14]. Atomic force microscopy (AFM) image (Inset Figure 2b) shows that the thickness of the CrTe nanoflake is down to ~5 nm. Figure 2c shows the morphology of CrTe nanoflake on the Cu grids which transferred *via* poly-(methyl methacrylate) (PMMA) assisted method. Scanning transmission electron microscopy (STEM) was introduced to further investigate the crystal structure and quality of the CrTe nanoflakes. The STEM image (Figure 2d) demonstrated that the crystal lattice spacing of as-synthesized CrTe nanoflakes was 0.34 nm, which attributed to the (100) planes of hexagonal-phase CrTe. The corresponding line intensity profile was shown in Figure S1.The elemental mapping (Figure 2e, f) demonstrate that Cr and Te element are evenly distributed in the sample. Energy dispersive spectroscopy (EDS) analysis (Figure 2g) was used to verify the elemental composition of CrTe nanoflakes, showing that the samples were consisted by Cr and Te atoms. Furthermore, the X-ray photoelectron spectroscopy (XPS) were used to confirm the chemical bonds composition of the CrTe samples. The high-resolution XPS survey of Cr 2p and Te 3d are shown in Figure 2h-i. Actually, the binding energies of Cr 2p and Te 3d are very close to each other. The peaks at 583.9

and 574 eV are stemmed from Cr $2p_{1/2}$ and Cr $2p_{3/2}$, while the peaks at 585.3 and 574.9 eV are related to Te $3d_{3/2}$ and Te $3d_{5/2}$, respectively. In addition, the XRD pattern (Figure S2) of our sample is matched to the NiAs structure CrTe pattern (PDF#97-009-3160). The results of Raman, STEM, EDS, XPS and XRD analysis confirmed that the as-synthesized nanoflakes were CrTe. In additoin, the thickness of the CrTe nanoflakes can be controlled by the growth time. **Figure 3**a-c shows the optical images of the CrTe nanoflakes synthesized in different reaction time of 5, 10, 15 min. By increasing the reaction time, the thickness of CrTe nanoflakes increases appreciably, which is about 14 nm, 19 nm and 27 nm, respectively. The corresponding atomic force microscopy (AFM) images of the CrTe nanoflakes were shown in Figure 3d-f. Furthermore, the thickness-dependent Raman spectra was shown in Figure S3. The peak at 123 cm^{-1} shows a blueshift with thickness increases, which may be attributed to Coulombic interactions and changes in intralayer bonding [23].

In order to investigate the effects of the Te powder in the mixed compounds on the synthesis of CrTe, the weight ratio of Cr: $CrCl_3 \cdot 6H_2O$: Te were adjusted to 1:1:0, 1:1:0.5, 1:1:1, 1:1:2. All the experiments were performed at 700°C for 5 min of growth. The optical images of CrTe samples grown at various weight ratios of mixed compounds are shown in **Figure 4**. The corresponding histogram statistics of the lateral dimension distribution of CrTe are shown in Figure S4. From the results, only several small CrTe nanoflakes (~6 μm) can be observed when Te powder was not involved in the mixed compounds, which is shown in Figure 4a. However, the size of CrTe nanoflakes increase remarkably when Te powder was introduced in the mixed compounds. The proportional relation between the size of as-synthesized CrTe nanoflakes and the weight ratio of Te powder in the mixed compounds can be explained by the enhanced mass flux of Cr precursor. At a certain vapor pressure (fixed reaction temperature, reaction time and gas flow rate), mass flow rate affects the nucleation rate and the growth rate, which has been reported by Zhu [24]. The participation of Te powder in the mixed compounds lower the melting point of the mixed compounds, which promotes faster evaporation of the metal precursors. Then the mass flow of metal precursor increased and promoted the nucleation and growth of CrTe on SiO_2/Si

substrate. Therefore, large-scale CrTe nanoflakes can be successfully synthesized.

Conclusion

In summary, the large-scale and high quality CrTe nanoflakes were synthesized on SiO_2/Si substrates by using CVD system. The Te powder in metal precursors is conducive to the growth of large-scale CrTe nanoflakes. The as-synthesized CrTe nanoflakes exhibit the largest domain size of ~250 μm on SiO_2/Si substrate. Meanwhile, the thickness of CrTe nanoflakes can be controlled by changing growth time. Our work demonstrated an effective pathway to grow large-scale 2D transition metal tellurides.

Experimental Section

CVD growth of CrTe nanoflakes: CrTe nanoflakes were synthesized inside a tube furnace (Lindberg/Blue M) equipped with a 1.2-metre length and 1 inch. diameter quartz tube in an ambient pressure CVD system. Te powder (99.997%, Sigma Aldrich) was used as Te precursor. The mixed compounds of Cr (99%, Sigma Aldrich), $CrCl_3$•$6H_2O$ (98%, Aladdin) and Te powder were used as metal precursor. In a typical experiment, the excessive Te powder was placed in a quartz boat and located upstream of the hot zone away from the metal oxide precursors. The mixed precursor (Cr: $CrCl_3$•$6H_2O$: Te = 1:1:2) was placed in the ceramic boat and placed in the center of the tube. The SiO_2/Si substrate was placed on the boat with the surface downside. Before the heating process, the furnace was purged by flowing 300 sccm high-purity Ar gas for 5 min. The center of furnace was heated to 700°C at a ramp rate of 25°C min^{-1}. The growth was conducted at 700°C with 100 sccm Ar for 2 min. After synthesis, the furnace was cooled down naturally to room temperature.

Materials characterizations: The as-obtained CrTe nanoflakes were further characterized by optical microscopy (Olympus BX53M), Raman (WITEC alpha 300R Confocal Raman system using a 532 nm laser as the excitation source), Atomic force microscopy (AFM, Asylum Research Cypher Scanning Probe Microscope system with a tapping mode) and X-ray photoelectron spectroscopy (XPS, ESCALAB 250 Xi). The STEM samples were prepared with a poly(methyl methacrylate) (PMMA) assisted method. The SiO_2/Si with CrTe nanoflakes on top was first spin-coated with a layer of

PMMA and then baked at 180 °C for 3 min. Subsequently, the wafer was immersed in NaOH solution (1M) to etch away the SiO_2 layer. After lifting off, the PMMA/CrTe flakes was transferred into deionized (DI) water to wash away the residual Na^+ ions and later moved to a TEM grid. The transferred sample was left to dry naturally and then put into acetone solution overnight to get rid of the PMMA coating entirely. An aberration-corrected Nion UltraSTEM-100 operating at 100 kV was used to obtain the STEM imaging.

Acknowledgements

This work was supported by the National Research Foundation–Competitive Research Program of Singapore NRF-CRP21-2018-0007 and CRP22-2019-0060, MOE Tier 2 MOE2017-T2-2-136, Tier 3 MOE2018-T3-1-002, and A*Star QTE programme. The National Natural Science Foundation of China (grants 61974120), the Key Program for International Science and Technology Cooperation Project of Shaanxi Province (grants 2018KWZ-08 and 2019KW-029).

Conflict of Interest

The authors declare no conflict of interest.

References

[1] B. Radisavljevic, M.B. Whitwick, A. Kis, ACS Nano, **2011**, *5*, 9934–9938.

[2] H. Tian, M. L. Chin, S. Najmaei, Q. Guo, F. Xia, H. Wang, M. Dube, Nano Res., **2016**, *9*, 1543–1560.

[3] A. Ramadoss, T. Kim, G. Kim, S. J. Kim, New J. Chem. **2014**, *38*, 2379–2385.

[4] H. Medina, J. Li, T. Su, Y. Lan, S. Lee, C. Chen, Y. Chen, A. Manikandan, S. Tsai, A. Navabi, X. Zhu, Y. Shih, W. Lin, J. Yang, S. R. Thomas, B. Wu, C. Shen, J. Shieh, H. Lin, A. Javey, K. L. Wang, Y. Chueh, Chem. Mater. **2017**, *29*, 1587−1598

[5] Y. He, P. Tan, Z. Hu, Q. He, C. Zhu, L. Wang, Q. Zeng, P. Golani, G. Gao, W. Fu, Z. Huang, C. Gao, J. Xia, X. Wang, X. Wang, C. Zhu, Q. M. Ramasse, A. Zhang, B. An, Y. Zhang, S. Martí-Sánchez, J. R. Morant, L. Wang, B. K. Tay, B. I. Yakobson, A. Trampert, H. Zhang, M. Wu, Q. J. Wang, J. Arbiol, Z. Liu. Nat. Commun., **2020**, *11*, 57.

[6] J. Lee, S. Lee, J. H. Ryoo, S. Kang, T. Y. Kim, P. Kim, C. Park, J. Park, H. Cheong,

Nano Lett. **2016**, *16*, 7433.

[7] X. Wang, K. Du, Y. Y. F. Liu, P. Hu, J. Zhang, Q. Zhang, M. H. S. Owen, X. Lu, C. K. Gan, P. Sengupta, C. Kloc, Q. Xiong, 2D Mater. **2016**, *3*, 031009.

[8] C. Gong, L. Li, Z. Li, H. Ji, A. Stern, Y. Xia, T. Cao, W. Bao, C. Wang, Y. Wang, Z. Q. Qiu, R. J. Cava, S. G. Louie, J. Xia, X. Zhang, Nature, **2017**, *546*, 265.

[9] B. Huang, G. Clark, E. Navarro-Moratalla, D. R. Klein, R. Cheng, K. L. Seyler, D. Zhong, E. Schmidgall, M. A. McGuire, D. H. Cobden, W. Yao, D. Xiao, P. Jarillo-Herrero, X. Xu, Nature, **2017**, *546*, 270.

[10] S. Jiang, J. Shan, K. F. Mak, Nat. Mater. **2018**, *17*, 406.

[11] Y. Deng, Y. Yu, Y. Song, J. Zhang, N. Z. Wang, Z. Sun, Y. Yi, Y. Z. Wu, S. Wu, J. Zhu, J. Wang, X. H. Chen, Y. Zhang, Nature, **2018**, *563*, 94;

[12] Bonilla, M. S. Kolekar, Y. Ma, H. C. Diaz, V.r Kalappattil, R. Das, T. Eggers, H. R. Gutierrez, M. Phan, M. Batzill, Nat. Nanotechnol, **2018**, *13*, 289.

[13] D. J. O'Hara, T. Zhu, A. H. Trout, A. S. Ahmed, Y. K. Luo, C. H. Lee, M. R. Brenner, S. Rajan, J. A; Gupta, D. W. McComb, R. K. Kawakami, Nano Lett. **2018**, *18*, 3125.

[14] M. Wang, L. Kang, J. Su, L. Zhang, H. Dai, H. Cheng, X. Han, T. Zhai, Z. Liu, J. Han, Nanoscale, **2020**, *12*, 16427.

[15] Z. Zhang, J. Niu, P. Yang, Y. Gong, Q. Ji, J. Shi, Q. Fang, S. Jiang, H. Li, X. Zhou, L. Gu, X. Wu, Y. Zhang, Adv. Mater. **2017**, *29*, 1702359.

[16] J. Li, B. Zhao, P. Chen, R, Wu, B. Li, Q. Xia, G. Guo, J. Luo, K. Zang, Z. Zhang, H. Ma, G. Sun, X. Duan, X. Duan, Adv. Mater. **2018**, *30*, 1801043.

[17] W. Ge, K. Kawahara, M. Tsuji, H. Ago, Nanoscale, **2013**, *5*, 5773.

[18] S. Zhao, T. Hotta, T. Koretsune, K. Watanabe, T. Taniguchi, K. Sugawara, T. Takahashi, H. Shinohara, R. Kitaura, 2D Mater. **2016**, *3*, 025027.

[19] B. Zhao, W. Dang, Y. Liu, B. Li, J. Li, J. Luo, Z. Zhang, R. Wu, H. Ma, G. Sun, Y. Huang, X. Duan, X. Duan, J. Am. Chem. Soc. **2018**, *140*, 14217.

[20] J. Zhou, J. Lin, X. Huang, Y. Zhou, Y. Chen, J. Xia, H. Wang, Y. Xie, H. Yu, J. Lei, D. Wu, F. Liu, Q. Fu, Q. Zeng, C. Hsu, C. Yang, L. Lu, T. Yu, Z. Shen, H. Lin, B. I. Yakobson, Q. Liu, K. Suenaga, G. Liu, Z. Liu, Nature, **2018**, *556*, 355-359.

[21] Y. J. Gong, J. H. Lin, X. L. Wang, G. Shi, S. D. Lei, Z. Lin, X. L. Zou, G. L. Ye,

R. Vajtai, B. I. Yakobson, H. Terrones, M. Terrones, B. K. Tay, J. Lou, S. T. Pantelides, Z. Liu, W. Zhou, P. M. Ajayan, Nat. Mater., **2014**, *13*, 1135.

[22] J. Zhou, F. Liu, J. Lin, X. Huang, J. Xia, B. Zhang, Q. Zeng, H. Wang, C. Zhu, L. Niu, X. Wang, W. Fu, P. Yu, T. Chang, C. Hsu, D. Wu, H. Jeng, Y. Huang, H. Lin, Z. Shen, C. Yang, L. Lu, K. Suenaga, W. Zhou, S. T. Pantelides, G. Liu, Z. Liu. L, Adv. Mater. **2017**, *29*, 1603471.

[23] C. Lee, H. Yan, L. E. Brus, T. F. Heinz, J. Hone and S. Ryu, ACS Nano, **2010**, *4*, 2695-2700.

[24] D. Zhu, H. S., F. Jiang, D. Lv, V. Asokan, O. Omar, J. Yuan, Z. Zhang, C.Jin, npj 2D Materi. Appl., **2016**, *1*, 8.

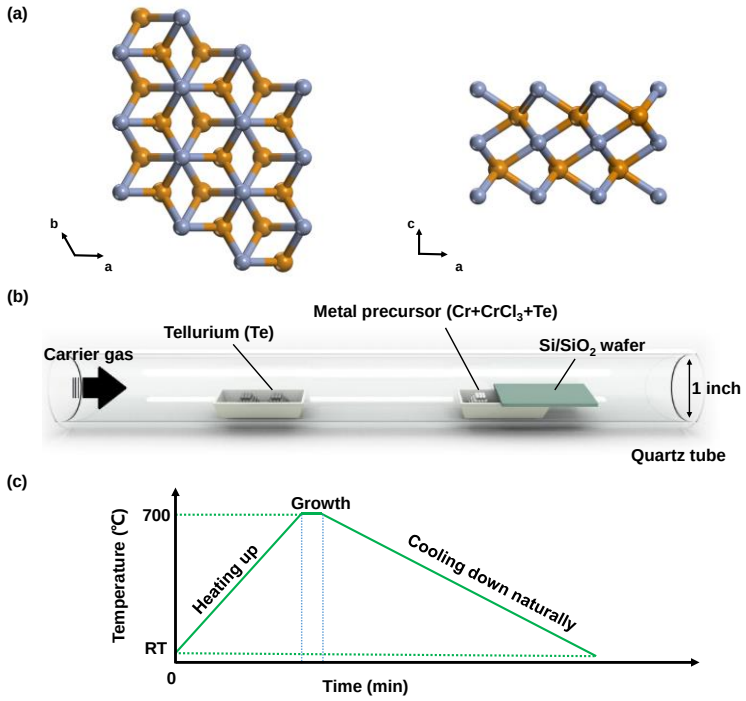

Figure 1 (**a**) Crystal structure diagrams of CrTe. (**b**) Schematic of the experimental setup to synthesize CrTe nanoflakes. (**c**) Temperature profile adopted in our experiments.

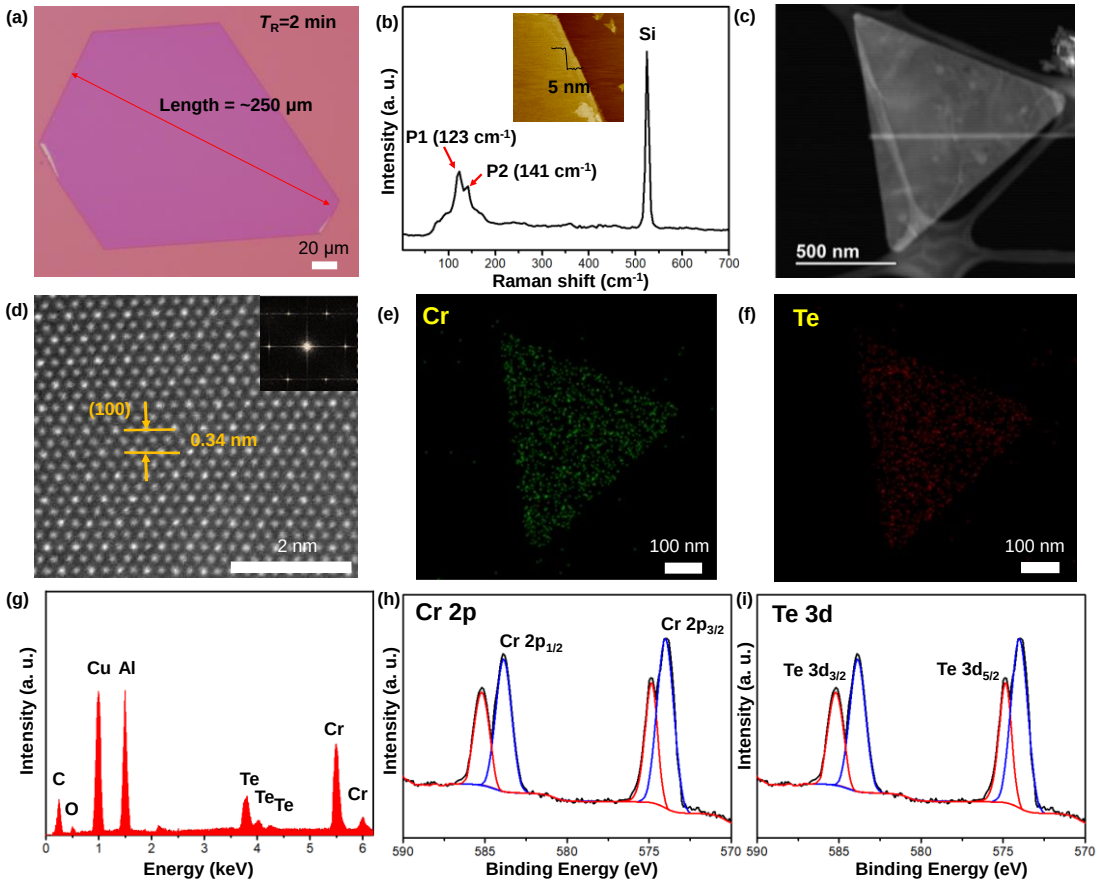

Figure 2 (a) optical images of the large CrTe nanoflake obtained in 2 min at 700 °C

with carrier gas of 100 sccm Ar/5 sccm H_2. (b) Raman spectra of the CrTe nanoflake (Inset: AFM image of the CrTe nanoflake), (c) Morphology of the transferred CrTe nanoflake on Cu grids. (d) High-resolution STEM image of the CrTe nanoflake (Inset: corresponding FFT pattern) (e, f) EDS mappings of elements Cr and Te. (g) The EDS elemental analysis of CrTe. (h-i) XPS characterization of Cr 2p and Te 3d spectra.

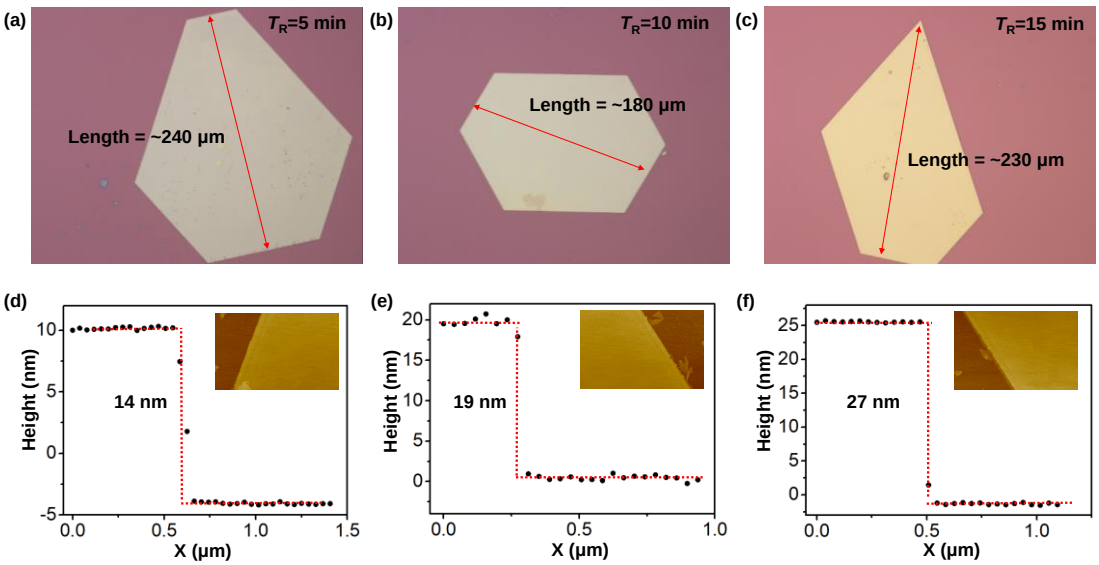

Figure 3 (**a-c**) Optical images of the CrTe nanoflakes synthesized at 700°C with growth time of 5, 10, 15 mins. (**d-f**) Corresponding AFM height profile and images.

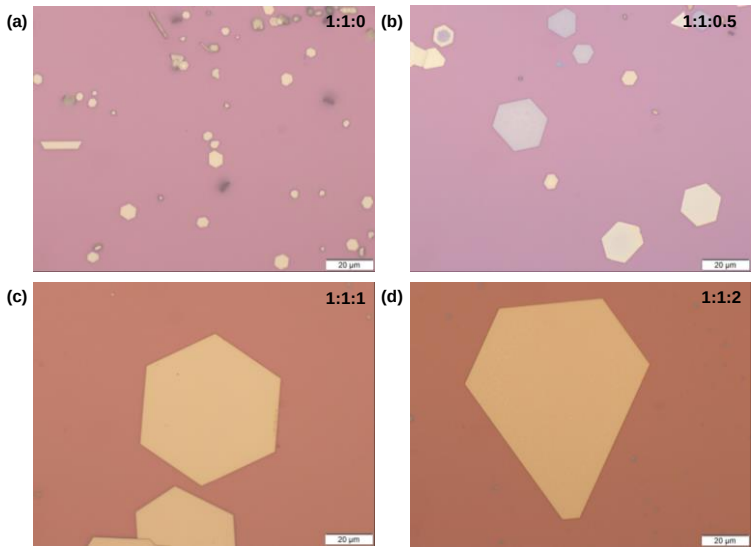

Figure 4 Optical images of the CrTe nanoflakes synthesized under various weight ratio of Cr: $CrCl_3 \cdot 6H_2O$: Te: (**a**) 1:1:0, (**b**) 1:1:0.5, (**c**) 1:1:1, (**d**) 1:1:2.